

Heat Transfer Characteristics Analysis of a Nanofluid in a Tube with a Co-axial Twisted Tape Inserter: A Numerical Approach

Tasnimul Alam*, Mohammad Ilias Inam

Department of Mechanical Engineering, Khulna University of Engineering & Technology, Khulna-9203, Bangladesh

Received: April 04, 2021, Revised: July 14, 2021, Accepted: July 18, 2021, Available Online: August 21, 2021

ABSTRACT

This study demonstrates the forced convection heat transfer of a water-based nanofluid inside a circular tube with a twisted tape inserter. During these simulations, it was assumed that the tube wall heated with constant heat flux, inlet of the tube had a lower temperature and Titanium Oxide (TiO_2) particles were used as nanoparticles for nanofluid mixture. The results depict the effect of some significant parameters, i.e., twist ratio (T.R.), number of twists, Reynolds number, and volume fractions of nanoparticles on the heat transfer characteristics inside the tube with a twisted tape inserter. It is visualized from the numerical results that the Nusselt number (Nu) and heat transfer co-efficient have higher values at the twisted region than the outlet. During this numerical simulation, the Reynolds number (Re), volume fractions of particles, and twist ratios were varied into the range from 100 to 500, 0 to 0.1, and 1 to 5, respectively. Mixture model conducted these numerical simulations with Direct Numerical Simulation (DNS) method using ANSYS Fluent 16.2 with the help of three-dimensional Navier-Stokes equation. The results depicted for both water and nanofluid, the average Nusselt number and heat transfer co-efficient enhance at lower twist ratios and a higher number of twists. Results also show that Nusselt number and heat transfer coefficient increase with Reynolds Number. The heat transfer characteristics of twisted-tape inserter portion and their differences of those characteristics with the tube outlet were investigated numerically and graphically.

Keywords: Twist Ratio, Volume Fraction, Reynolds Number, Nusselt Number, Heat Transfer Co-efficient, DNS.



This work is licensed under a [Creative Commons Attribution-Non Commercial 4.0 International License](https://creativecommons.org/licenses/by-nc/4.0/).

1 Introduction

Heat transfer is very common in lots of environmental and industrial applications. Due to that, lots of research have been conducted to enhance the convection heat transfer characteristics. Laminar flow heat transfer inside a circular tube is popular like in refrigeration and heat exchanger, just a name of a few. One of the most common heat enhancement procedures is to use twisted-tape in plain tubes. Bergles and Somerscales illustrated the enhancement of heat transfer by several active or passive methods. The author observed heat transfer enhancement by inserting a twisted-tape in laminar pipe flow [1]. Nanofluids' peristaltic motion through a porous medium that follows the non-Newtonian method inside the asymmetric channel was investigated by Eldabe and Abo Seida et al. [2]. Nanoparticles' effect on the heat transfer characteristics inside a circular tube is shown by Sundar et al. for different Reynolds numbers (Re) ranging 3000 ~ 22,000 and volume fractions of particles varying 0.1% ~ 0.3. The author found that Nusselt Number increased with Re and volume fraction; however, pumping power also increased by 18% with the volume fraction of particles [3]. Wie He and Davood Toghraie investigated the effect of a twisted tape inserter inside a tube considering the single-phase model and multiphase model. They found that multiphase models give closer results to actual results rather than using a single-phase model. They also found that twisted tape provides better performance. For instance, single tape provides 2.18 times, whereas twin twisted tape gives 2.04 times [4]. M. Arulprakasa et al. analyzed the effect of conical strips on the heat transfer characteristics using various twist ratios and geometrical configuration. The strips of the conical shape generate swirl flow which gives a higher Nusselt number as a result of higher fluid

mixing. This enhancement technique protects the matter of cost and plays an important factor in energy consumption. This passive technique decreases the thermal boundary layer, which intensifies fluid mixing [5]. S. Eiamsa-ard et al. illustrated the newly constructed DWTs regarding heat transfer enhancement devices. It was assumed that wing structural part situated near the wall enhanced the decisive point of heat transfer rate. Turbulence conducted in different experiments for three different types of twist ratios 3, 4 and 5. Here, the Reynolds numbers were varied 3,000 to 27,000. Oblique delta-winglet and straight delta-winglet arrangement were set up to investigate the heat transfer characteristics to a certain extent [6]. Yeping Ping et al. depicted an external magnetic field's influence in the convective nanofluid flow having an impact of heat dissipation and thermal radiation. A rotating tube with a low, stable angular velocity induced the forced flow incident while the outer circumference tube remained firm. Aspect ratio, Reynolds numbers, Hartmann numbers, and radiative parameters was measured in that numerical study [7]. Shyy Woei Chang, Ker-Wei Yu, Ming Hsin Lu examined the effect of heat transfer due to single, double, and triple twisted tape inside a hollow circular enclosure by numerical method. They illustrated all the calculations ranging Reynolds numbers from 3,000 to 14,000, and the Nusselt numbers 1.5-2.3, 1.98-2.8, 2.86-3.76 for single, double, and triple twisted tubes, respectively. They strategically aimed to focus on extending the Reynolds number in different circumstances. The clearance between the edges of the tube's tape, wall, and cyclic swirls' characteristics was maintained stable in twin, triple twisted-tapes inserting the tube [8]. S. Eiamsa-ard, K. Wongcharee, K. Kunrak, Manoj Kumar analyzed the behavior of a tube consisting dimples all over the surface and having a twisted tape inserting in it. The angles used

*Corresponding Author Email Address: rishan11bd@gmail.com

for dimples were 0, 15, 30, and 45 degrees; the twist ratios for calculation were 3.0, 4.0, 5.0 and volume fractions used for TiO₂ nanofluids were 0.05, 0.1, and 0.15%. This study covers Reynolds numbers ranging from 5,000 to 15,000. However, these dimple surface studies boosted up the blending of fluid, creating secondary flow and enhanced thermodynamic properties through the tube [9]. M. Jafaryar et al. investigated the characteristics of heat transfer using CuO-H₂O nanofluid consisting of a twisted-tape insert in a heat exchanger. This mixture's behavior was considered a single phase. The phenomena of better mixing of nanofluids were investigated by decreasing the pitch ratio. Mainly they work on the influence of swirling flow in nanofluid hydrodynamic nature [10]. The effect of a twisted perforated tape inserts having V cut configuration in a heat exchanger was investigated by Bipin Kumar, Manoj Kumar, Anil Kumar, and Siddhart Jain. They showed that heat transfer augmentation occurred varying the twist ratio 2 to 6, Reynolds number ranging from 2,700 to 23,400. This performance was measured at 1.58, where the V-cut and PTT pitch ratio changing from 1 to 2. In this case, the enhancement of heat transfer was measured by the minimum friction fall. As the PTT has the characteristics to enhance the heat transfer with less pressure drop compared to solid twisted tape (STT), hence it is proved convenient where V-cut twisted tape being used on the periphery of the structure [11]. J.P. Meyer, S.M. Abolarin investigated the heat transfer augmentation and the pressure drop characteristics in transition flow regime in a circular tube having a square-edged inlet and twisted tape inserts. The experiment was done using various twist ratios of 3, 4, and 5 where the square-edged configuration was used as the inlet. The tube has a constant heat flux confined in it. Reynolds numbers were ranged from 400 to 14,000, and the Prandtl number used in that changing between 2.9 and 6.7. When the twist ratio was kept constant, the heat flux varied. As the flux got higher, it delayed the transition from laminar to turbulent flow. If both the twist and Reynolds number had remained constant, an increment of heat flux would cause a decrease in friction factor values [12]. L. Syam Sundar et al. experimented the laminar convective heat transfer through a circular tube having a constant heat flux where Al₂O₃, TiO₂, and CuO nanofluids were used for investigating the thermodynamic properties of the flow, i.e., thermal conductivity, density and viscosity. This work had been investigated in a constant heat flux boundary condition. Moreover, each value had been compared with rational values, and the improvement in heat transfer was depicted [13]. The water flows having mixed with magnetite nanoparticles acquired two parallel disks that increase the thermal conductivity. This study is depicted by Rizwan Ul Ha1 et al. Magnetite (Fe₃O₄), Cobalt ferrite (CoFe₂O₄), and Mn-Zn ferrite (MnZnFe₂O₄) are mixed with water where water acted as the base fluid. All those results were investigated for velocity, temperature, reduced screen friction, and reduced Nusselt numbers. The variation in parameters enhances the thermal conductivity. In this investigation, water-based Magnetite (Fe₃O₄) gave the maximum lowest friction factor and low Nusselt number compared with the other mixtures. The temperature distribution was depicted broadly plotting against various nanofluid volume fractions to discuss this squeezing channel's full domain [14]. Ali Celen et al. explored a numerical method where the single-phase flow of base fluid water was compared and simulated with TiO₂ nanoparticles immersed in a base fluid with constant heat flux having temperature-dependent parameters. Local and average heat transfer characteristics such as pressure drop, temperature, and velocity distribution in several types of tested pipes were thoroughly investigated in this procedure. This study's results between measured values,

numerical outputs and their changes had been represented in terms of Reynolds number and flow rate [15]. The thermodynamic performance using nanofluid flow in a triangular tube consisting a twisted tape was discussed by Cong Qi, Maoni Liu, Tao Luo, Yuhang Pan, and Zhonghao Rao. The effect of nanoparticles in a tube having twisted tape was defined by mass fractions, in which cases 0.1 wt%, 0.3 wt%, and 0.5 wt % had been utilized, and the Reynolds number ranged (*Re*) 400-9000. They found a significant increment in Nusselt number by 52.5% and 34.7% for laminar and turbulent flow, respectively. The performances of heat transfer characteristics in both triangular and corrugated tubes were compared. However, it was revealed that the triangular tube with twisted tape has higher heat transfer performance than the corrugated tube [16]. Fatih Selimefendigi et al. analyzed the effect of conjugate natural convection where there was a cavity with a conductive partition. The nanofluids create the conductivity both of the opposite sides of the partitions. Al₂O₃, CuO nanoparticles were used on different sides of the partitions; a numerical analysis was performed by taking Grashof numbers 10³-10⁶, the angles of sloping between 0 to 275 degrees, thermodynamic conductivity ranged from 0.01 to 10, and finally, the volume fractions were used between 0 to 0.04. The investigation showed that thermodynamic conductivity increased due to the partitions. Simultaneously, the heat transfer rate increased its value for fulfilling the cavity with nanofluid particles [17]. Heat transfer characteristics of transient nanofluid flow between parallelly placed plates using magnetic field described in Buongiorno model were investigated by M. Sheikholeslami et al. The validation of this work was done by comparing with the results of viscous fluid. Hartmann number, Schmidt number, Brownian motion parameters, and Eckert number were used for calculating different analytical procedures in that regard. It was also revealed that the Nusselt number is enhanced by the enhancement of Hartmann number, Eckert number, and Schmidt number, but due to the increase of squeeze number, it decreases [18]. L. Syam Sundar et al. analyzed the impact of twisted tape in concern of heat transfer and friction factor improvement with Fe₃O₄ nanofluids, which reveal the magnetic characteristics. In the particular case the twist ratio (*y/d*) was taken ranging from 0 to 15, the Reynolds number varied from 3,000 to 22,000. Here, the friction factor faced increment due to 0.6% volume fraction of the nano particles' mixture. The analyzed results were compared with the generalized experimented results and found out that friction factor increment 1.231 times with Fe₃O₄ particles with base fluid [19]. The conduction and convection heat transfer nature of the Au-H₂O nanofluid mixture having differential with walls in a cubic confined system or enclosure had been depicted by Primoz Ternik et al. The confined walls were presumed to be adiabatic. The standard finite volume method and Boussinesq approximation were utilized to solve the differential governing equations for each case. Volume fractions were taken 0 to 5% in this regard, and Rayleigh's ranged from 10¹ to 10⁶. The Nusselt number faced decrement while the volume fractions were greater than 0% [20]. The capability of heat transfer through a medium where pressure drop occurs and plays a significant role with multiple twisted tape inserts in a circular enclosure was investigated by Chaitanya Vashistha et al. The technique reduced the cost and enhanced heat transfer characteristics. Having used single, twin, four twisted tape with twist ratios 2.5, 3, and 3.5 for swirl and counter swirl flow, using the Reynolds number ranging from 4,000 to 14,000, they found out that the maximum heat transfer is possible due to the value of twist ratio 2.5 with the rise of friction losses. The maximum rise had been found for heat transfer and friction factor 2.42 and 6.96 correspondingly with

the comparison of smooth tube performance, and it was discussed by the characteristics of flow patterns [21]. Zeinali et al. investigated the heat transfer of Al_2O_3 -water nanofluid flow through a duct that assimilates at the cross-section. There was seen a high-pressure fall, high-pressure trial structure where the fluid flow characteristics have been measured. Still, the square section provides a minimum pressure drop and a better heat augmentation performance illustrated in this particular technique. However, the heat exchange rate was not well enough if a circular duct used in such case for enhancement, nanofluid flow through a changed geometrical structure could be optimum to heat transfer enhancement. Using the different configurations, the enhancement of the heat transfer coefficient was 27.6% utilizing 2.5% volume fractions of nanoparticles [22]. The mixed fluid flow that is fully developed through an inclined and horizontal tube having a heat flux with uniform rate heat transfer performance was measured by M. Akbari et al. The fluid flow characteristics with an extended range of Reynolds number and Grashof had been used to solve the three-dimensional governing equations in that case. The impact of nanoparticles and the quantity of inclination in heat transfer performance has been illustrated and represented in this technique. The study showed that maximum heat transfer could be gained by 15% using 4% volume fractions of Al_2O_3 and the slope was 45 degrees for inclination [23]. M.M Rashidi, Mohammad Nasiri, Marzieh Khezerloo, and Najib Laraqi investigated the impact of a magnetic field in heat transfer characteristics of nanofluid flow where mixed convection was present. The vertical channel having sinusoidal walls where the numerical study has proceeded. In that case, the Nusselt number varied from 500 to 1000, three Hartman numbers 0, 5, and 10, sine waves having amplitude 0.1, 0.2, and 0.3 were taken to conduct the numerical study. Al_2O_3 nanofluid mixture was considered two dimensional and laminar, steady and incompressible flow. The thermal properties were assumed constant, and Boussinesq assumptions had been calculated by the density variation. It was revealed that with the increase of Grashof number, the Nusselt number enhances with various volume fractions of nanoparticles. Moreover, the Hartman number increases both the Nusselt and Poiseuille parameters that were also proved by Weres numerical investigation [24]. Ramtin Barzegian, Mostafa Keshavarz, and Alireza Alouyan experimented with the heat transfer characteristics and dropped pressure using TiO_2 nanofluid flow through a brazed plate heat exchanger (BPHE). The particles' size volume fractions 0.3%, 0.8%, and 1.5% were taken, where the investigation was fully done under turbulent flow conditions. The investigation showed that the heat transfer coefficient increases due to varied volume fraction particles with 99% pure distilled water. The maximum enhancement of the parameter i.e. heat transfer co-efficient for 0.3%, 0.8% and 1.5% volume fractions were examined 6.6%, 13.5% and 23.7% respectively. Further, it was revealed that there is a negligible increment of pressure drop compared to the enhanced heat transfer coefficient [25]. Thermoplastic properties for superheated steam were investigated by Fengrui et al., where a mathematical model is assumed to predict pressure and temperature in SHS injection wells. After the validation of the model, superheated degree at the bottom-most section increased; this parameter also increased by injection rate and injection temperature. The numerical study of intrinsic flow characteristics of SHS in the wellbore could be beneficial in the oil field [26]. The neural network numerical study with TiO_2 nanofluids having spirally coiled tube and magnetic field had been studied by P. Naphon, S. Wiriyasart, and T. Arisariyawong. Different training algorithms were utilized to solve errors for attaining the required ANN configuration.

Among those algorithms, Levenberg-Marquardt back propagation gives the optimal result. It was explored that for the required ANN model, the data falls within 2.5 to 5% variation of the heat transfer characteristics parameters, i.e., Nusselt numbers, friction factors. The optimal ANN had been applied to investigate the spirally coiled tube with the magnetic field's help [27]. Omid Ali Akbari et al. investigated the impact of velocity in the non-Newtonian fluid using base fluid nanoparticles. Carbon Methyl Cellulose (CMC) solution has a 5% weight concentration with water used as a base fluid using base fluid nanoparticles. A two-dimensional microchannel with Reynolds numbers ranging from 10 to 1000 and a cartesian model system was introduced. The non-Newtonian fluid motion creates effect on pressure drop, Nusselt number, temperature, and non-Newtonian fluid's motions, which were discussed elaborately in the numerical study. The analysis depicted that the increment in volume fractions and the decline in the particles' size enhanced the heat transfer performance [28]. The assumptions of heat transfer augmentation and pressure drop were investigated by Halit Bas and Veysel Ozceyhan by the method of Taguchi. The construction parameters i.e. twist ratio ($y/d = 2, 2.5, 3$ and 3.5), Reynolds number ($Re=5,200, 9,600, 14,000$ and $18,400$) were taken to analyze the effect of Nusselt numbers and pressure drop on such parameters. The motive of that numerical study was to define the reason for acquiring the highest Nusselt number and lowest pressure drop by performing the least number of experiments and reducing the cost. This method showed the pressure drop decreases with the increased twist ratio, Reynolds number, and clearance ratio [29]. A numerical approach in the nanofluid simulation was studied by Adriana Minea et al., which illustrated that nanofluid affected solar energy technology. In this approach, different procedures were introduced to investigate CFD analysis. The exact procedure was a considerable reference for analyzers who are likely to deal with the study regarding nanofluid flow [30]. The convective heat transfer characteristics of nanofluid flow for the cooling operation of electro-mechanical devices by the use of single-phase fluid flow was analyzed by Mangal Singh Lodhi et al. In this case, Al_2O_3 nanofluid laminar flow, Reynolds number ranging from 300 to 1000, particles' concentration 1.0 to 3.0 and the micro-channel having 500 μm inner diameter, length of 100 mm were assumed. The performance characteristics were compared with distilled water. They measured that the heat transfer co-efficient increment was up to 24.5% while the friction factor was achieved 22.7% higher than the regular value. The performance evaluation showed that the categorization of using this nanofluid flow having higher efficiency than unity ($\eta > 1$) [31].

The present paper studied the heat transfer characteristics, i.e., Nusselt number, heat transfer coefficient, the pressure drop in terms of different parameters i.e. Reynolds number, Twist ratio, number of twists, and volume fractions. However, a special case had not been discussed in the past studies of this field which is about the changes of the twisted inserter's heat transfer characteristics. Previously, all the reviews were about the outlet heat transfer characteristics, i.e., Nusselt number, Reynolds number, and pressure drop of a plain tube, rectangular or triangular channel. But in the present study, it can be seen the change of those characteristics in the twisted tape inserter having constant heat flux overall the circular tube. For calculating both the outlet and twisted tape portion's heat transfer characteristics, isosurfaces were created in both at the outlet of the tube and the end of the twisted inserter end. Thus, planes are created in both sections. Then again by using isosurface command and selecting fluid domain simultaneously in the setup portion of Ansys 16.2, we can calculate Nusselt number and heat transfer co-efficient

easily both at the outlet of tube and end of the twisted tape inserter. Different lengths of twisted tape inserters have been considered. However, the diameter of the inserters were fixed in all cases and twist-ratios were 1, 2, 3, 4 and 5. Further explanations of parameters have been discussed in section 3. Mainly this article focuses on the change heat transfer characteristics at the end of the twisted-tape inserter portion and the comparison of inserter's end to the outlet characteristics. TiO₂ nanoparticles mixture and water have been for individual calculations. And a comparison between water and nanofluid flow heat transfer characteristics at the outlet and twisted part of the tube have been made and represented graphically.

This paper has organized boundary conditions at section 2; numerical methodology along with mesh dependency has been presented in section 3; results and discussion are analyzed at section 4 and section 5 is the conclusion.

2 Boundary Conditions

In this paper, a plain tube of length $L=0.5$ m, diameter $D=0.025$ m, (refer to Fig. 1) the twist having a length of 0.1 m, 0.15 m, 0.16 m, 0.20 m, and 0.30 m; the diameter of the twist, $d=0.02$ m, have been taken. The plain tube contains a constant heat flux around the whole body, equal to $q=300$ Wm⁻², and it was assumed that the inlet temperature to be 306 K. For the Reynolds number 100 to 500 taking the interval of 100, the velocities were measured 0.004019, 0.008038, 0.0120577, 0.0160769 and 0.02009617 respectively. The initial gauge pressure is considered 0 Pascal in every condition. The heat transfer characteristics, i.e., Nusselt number, heat transfer coefficient, and pressure drop for the outlet and the twisted section, will be presented in this paper for twist-ratio (T.R.) 1, 2, 3, 4 and 5 as shown in Fig. 2-Fig. 6. The effect of the number of twists (1, 2, 3, 4, and 5) on heat transfer characteristics for a fixed length of twisted tape has also been investigated. The Nusselt number, heat transfer coefficient at the outlet for a plain tube having twisted tape inserter were measured separately both for water and TiO₂+water nanofluid flow varying Reynolds number from 100 to 600. The difference in those parameters for at the outlet wall and twisted tape inserter portion has also been analyzed. The twisted-tape has an adiabatic, no-slip condition, and the entrance length was considered sufficiently large for fully developed flow.

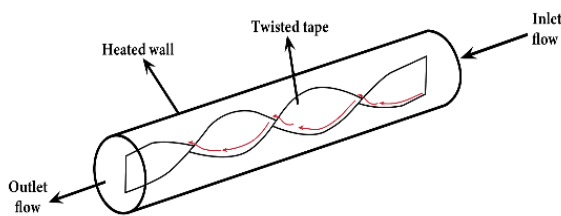


Fig. 1 Twisted-tape insert in a plain tube

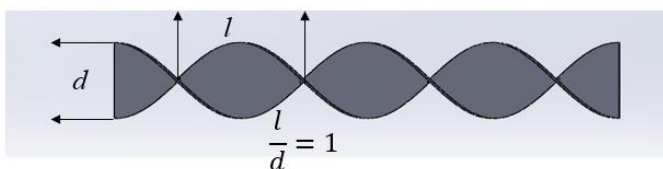


Fig. 2 Twisted-tape with twist-ratio (T.R.) 1

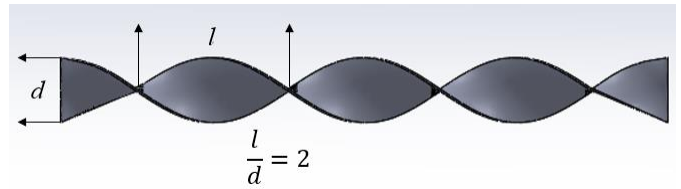


Fig. 3 Twisted-tape with twist-ratio (T.R.) 2

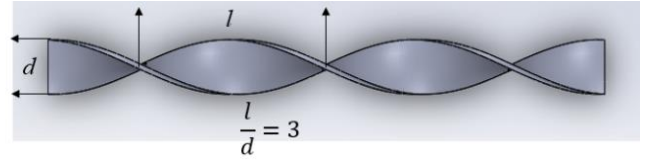


Fig. 4 Twisted-tape with twist-ratio (T.R.) 3

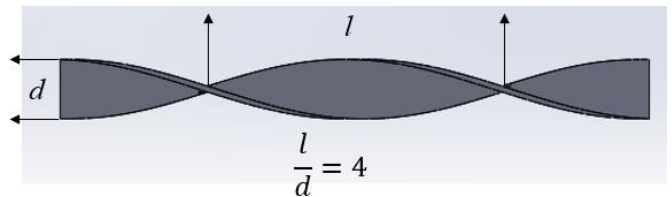


Fig. 5 Twisted-tape with twist-ratio (T.R.) 4

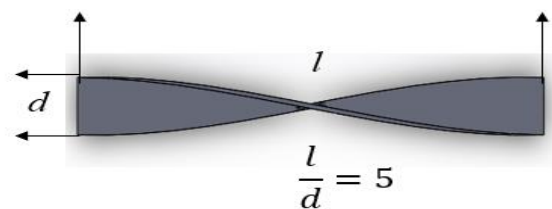


Fig. 6 Twisted-tape with twist-ratio (T.R.) 5

3 Methodology

3.1 Governing equations

The governing equations are continuity, momentum, and energy equations. Those equations are described as follows [32]

Continuity equation:

$$\frac{\partial U_x}{\partial x} + \frac{\partial U_y}{\partial y} + \frac{\partial U_z}{\partial z} = 0 \quad 1$$

The general energy condition is additionally called the condition of movement or Navier-Stoke's condition; moreover, the condition is often used in forced convection. The condition of coherence is grown just by applying the law of preservation of mass to a little volume component inside a streaming liquid.

Momentum equation:

X-momentum equation:

$$U_x \frac{\partial U_x}{\partial x} + U_y \frac{\partial U_x}{\partial y} + U_z \frac{\partial U_x}{\partial z} = -\frac{1}{\rho} \frac{\partial p}{\partial x} + \vartheta \left(\frac{\partial^2 U_x}{\partial x^2} + \frac{\partial^2 U_x}{\partial y^2} + \frac{\partial^2 U_x}{\partial z^2} \right) \quad 2$$

Y-momentum equation:

$$U_x \frac{\partial U_y}{\partial x} + U_y \frac{\partial U_y}{\partial y} + U_z \frac{\partial U_y}{\partial z} = -\frac{1}{\rho} \frac{\partial p}{\partial y} + \vartheta \left(\frac{\partial^2 U_y}{\partial x^2} + \frac{\partial^2 U_y}{\partial y^2} + \frac{\partial^2 U_y}{\partial z^2} \right) \quad 3$$

Z-momentum equation:

$$U_x \frac{\partial U_z}{\partial x} + U_y \frac{\partial U_z}{\partial y} + U_z \frac{\partial U_z}{\partial z} = -\frac{1}{\rho} \frac{\partial p}{\partial z} + \vartheta \left(\frac{\partial^2 U_z}{\partial x^2} + \frac{\partial^2 U_z}{\partial y^2} + \frac{\partial^2 U_z}{\partial z^2} \right) \quad 4$$

The entire domain is solved with a single momentum equation and the resulting velocity is shared between the phases. Those momentum equations in three dimensional volume (x, y and z) are dependent on the surface forces and body forces acting on the fluid. Surface forces act due to pressure and viscous stress whereas the body forces are determined by a generic body per unit volume integrated over the volume.

Energy equation:

$$U_x \frac{\partial T}{\partial x} + U_y \frac{\partial T}{\partial y} + U_z \frac{\partial T}{\partial z} = \frac{k}{\rho c_p} \left(\frac{\partial^2 T}{\partial x^2} + \frac{\partial^2 T}{\partial y^2} + \frac{\partial^2 T}{\partial z^2} \right) \quad 5$$

In this equation, x, y and z are spatial coordinates of a domain i.e. independent variables and density (ρ), temperature (T) are dependent of the independent variables. U_x , U_y and U_z are the velocity components of in x,y and z directions. Therefore, the equations are partial differential equations not the ordinary differential equations. In Ansys 16.2, the energy equation is kept on before running all whole calculations.

Thermoplastic properties of nanofluids can be measured by the following equations [33] -

Density for nanofluid:

$$\rho_{nf} = (1 - \varphi) \rho_w + \varphi \rho_{np} \quad 6$$

ρ_w = density of water

ρ_{np} = density of nanoparticle

φ = volume fraction of particle

Specific-heat of nanofluid:

$$C_{p,nf} = \frac{\varphi \rho_{np} C_{p,np} + (1-\varphi) \rho_w C_{p,w}}{\rho_{nf}} \quad 7$$

$C_{p,np}$ = specific-heat of nano particle

$C_{p,w}$ = specific-heat of water

Thermal conductivity of nanofluid:

$$\frac{k_{nf}}{k_w} = \frac{k_{np} + 2k_w + 2\varphi(k_{np} - k_w)}{k_{np} + 2k_w - \varphi(k_{np} - k_w)} \quad 8$$

k_w = thermal conductivity of water

k_{np} = thermal conductivity of nanoparticle

The viscosity of nanofluid:

$$\mu_{nf} = (1 + 2.5\varphi) \mu_w \quad 9$$

μ_w = viscosity of water

Here, the density (ρ_{nf}), specific heat capacity ($C_{p,nf}$) of TiO₂ nanofluid have been calculated based on the empirical correlations proposed by M. Hatami, A. Kheirkhah, H.Ghanbari-Rad, Dengwei Jing et al. Also, thermal conductivity (K_{nf}) and viscosity (μ_{nf}) for nanofluid have been estimated based on the semi-empirical equations presented by Teknik, Primož et al [20]. There are some equations needed to calculate the parameters of heat transfer augmentation. They are [34] -

$$Nu = \frac{hD}{k} \quad 10$$

Nusselt number is a dimensionless parameter defined by the ratio of convective heat transfer to conductive heat transfer.

$$Re = \frac{\rho VD}{\mu} \quad 11$$

Reynolds numbers help to predict the flow pattern. In this paper laminar flow of fluid is considered. So, the Reynolds number for plain tube flow is assumed lower.

$$Q = hA(T_w - T_f) \quad 12$$

This is the basic energy balance equation for convective heat transfer. Heat transfer mainly depends on the difference of the temperature of fluid outside the thermal boundary layer T_f and

the temperature of fluid on the surface T_w . Augmentation happens if heat transfer co-efficient (h) and surface area (A) increases.

$$q_1 = h\Delta T \quad 13$$

As the plain tube contains constant heat flux, the heat transfer coefficient, and the temperature difference ΔT are used to measure the parameter.

$$q_2 = h_{twist} \Delta T_{LMTD} \quad 14$$

This equation is required for calculating the heat transfer co-efficient in the twisted-tape (h_{twist}) from the constant heat flux previously discussed and ΔT_{LMTD} .

$$LMTD = \frac{(HT_s - CT_e) - (HT_e - CT_s)}{\ln\left(\frac{HT_s - CT_e}{HT_e - CT_s}\right)} = \frac{\Delta T_1 - \Delta T_2}{\ln\left(\frac{\Delta T_1}{\Delta T_2}\right)} \quad 15$$

$LMTD$ = log mean temperature difference

HT_s = hot stream starting temperature

HT_e = hot stream ending temperature

CT_s = cold stream starting temperature

CT_e = cold stream ending temperature

In the twisted section, there two isosurfaces were taken at the starting and end of the twist. From Ansys 16.2, the $LMTD$ can be calculated by taking the individual temperatures from the isosurfaces. Thus, the other parameters, i.e., Nusselt number and heat transfer of the twisted-tape, can be investigated.

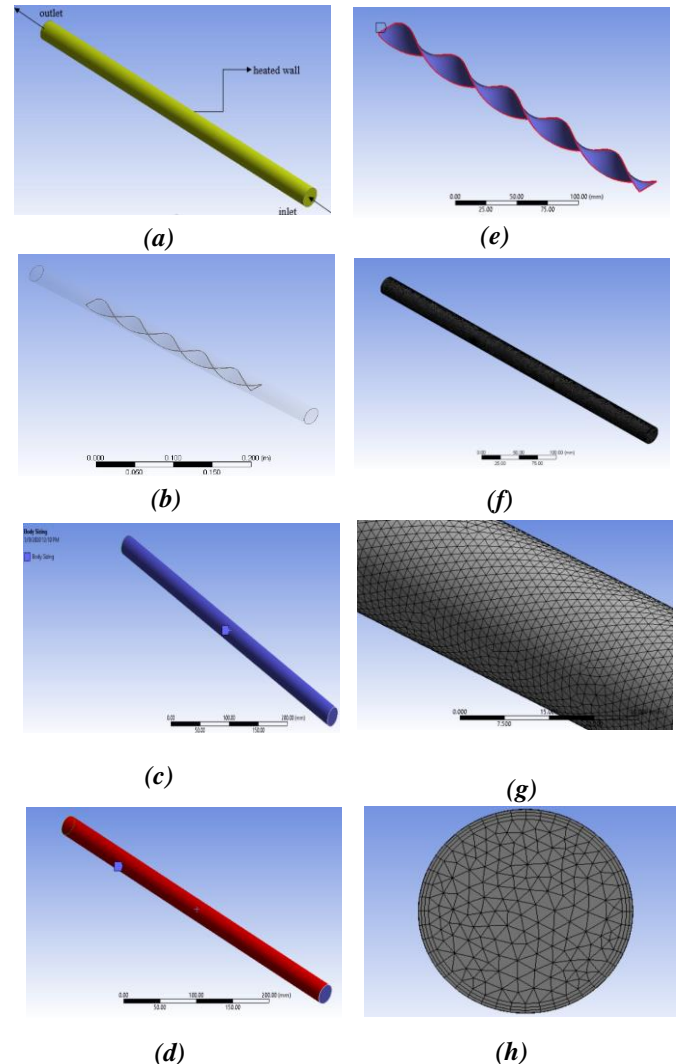
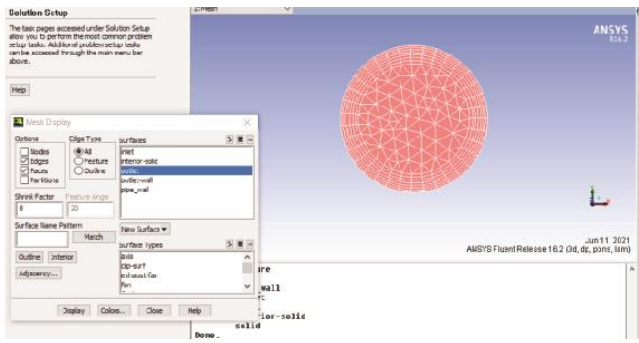
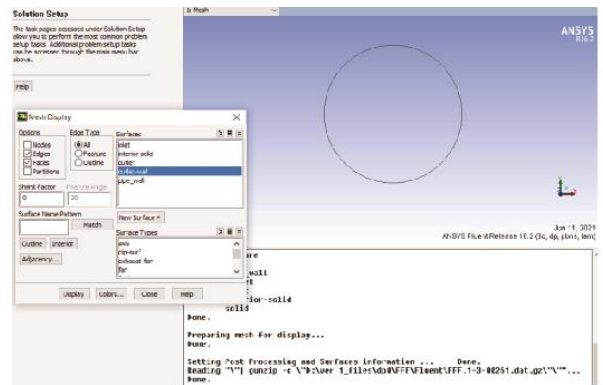


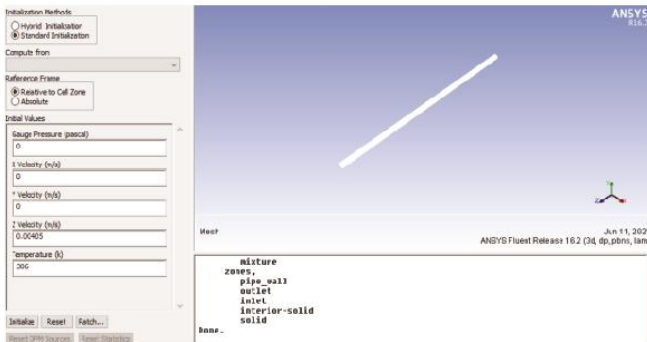
Fig. 7 Geometry and Mesh generation



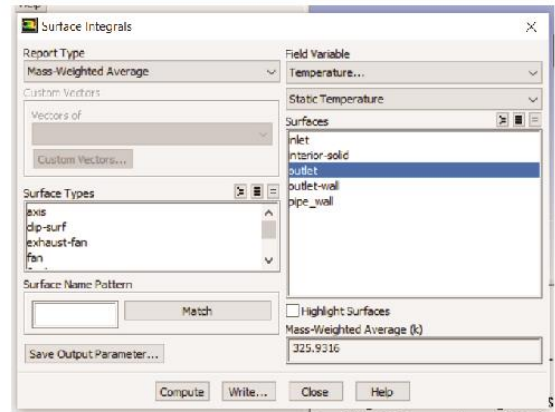
(a) Outlet



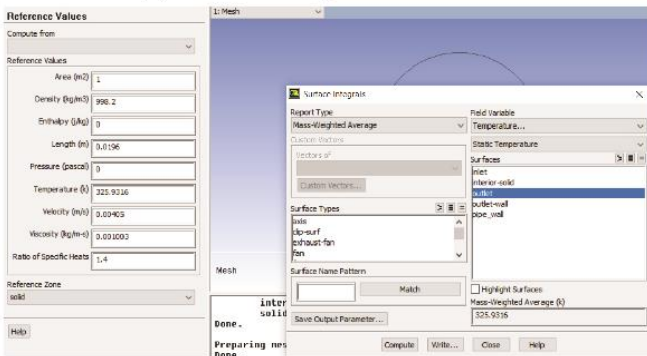
(b) Outlet Wall



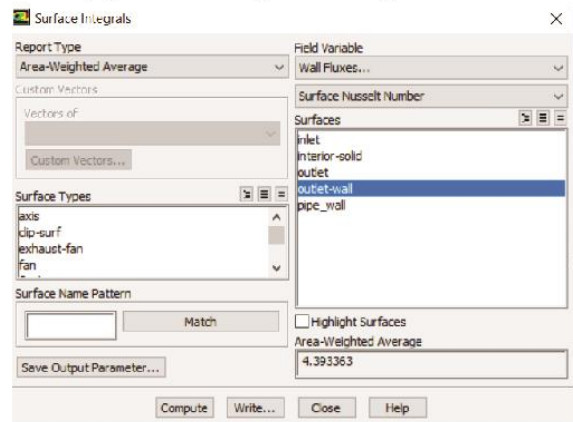
(c) Initial Temperature value



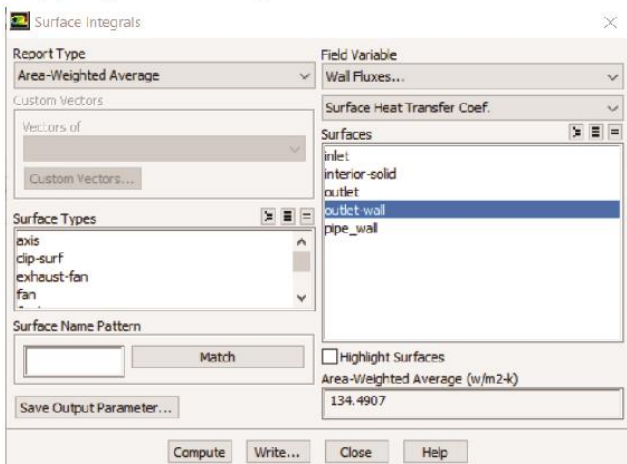
(d) Mass Weighted Temperature



(e) Reference temperature value at outlet wall



(e) Nusselt Number Calculations



(g) Surface heat transfer co-efficient

Fig. 8 Nusselt Number and Heat Transfer Co-efficient Calculation

Another vital formula that is required for observing in which length the fully developed flow occurs is "Entrance Length Formula" for laminar flow-

$$L_{h,laminar} = 0.05ReD \quad 16$$

Table 1 Thermoplastic properties of the base fluid and nanofluid particles [35]

Property	Water	TiO ₂
Density (Kgm ⁻³)	998.2	3985
Specific heat (Jkg ⁻¹ K)	4182	683
Thermal Conductivity (Wm ⁻¹ K ⁻¹)	0.60	11

3.2 Geometry and meshing

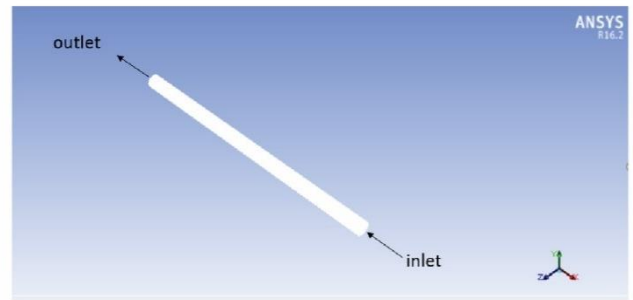
From Fig. 7, the different steps from geometry to mesh generation have been depicted by sub-figures (a) to (h). At first, the twisted-tape was created by SOLIDWORKS 18 software that has been imported at the geometry section of ANSYS 16.2 software, and an enclosure of cylindrical shape has been created that is shown in (a) whilst the following subsidiary figure (b) illustrated the existence of the twisted-tape inside the plain tube. Before finishing the geometry, the Boolean operation tool was utilized without preserving the tool body. Completing the first step in ANSYS, i.e., Geometry, (c) body sizing has been done by taking the element size of 1.8 mm in the second step, i.e., mesh section. An inflation layer has been imposed on the surface body, i.e., (d) of the tube. As laminar flow is considered in the whole operation, three layers of inflation operation has been taken in that option that is existed in the software. The subsectional figure (e) depicted that the inflation layer had been used at the eight different edges of the twist, taking three inflation layers as before. By clicking the option generate mesh, the final mesh product has been shown in (f) and (h) figures, revealing the mesh generation's close view. In subsidiary fig (f), the whole domain section shows a smooth transition. Another critical factor is that the growth rate has always been 1.2 in meshing operations. Several elements and element metrics statistics would be easily analyzed that the meshing operation was competent for this geometrical structure.

3.3 Procedure of Measuring Nusselt Number and Heat Transfer Co-efficient at the Outlet Wall and Twisted Tape Inserter

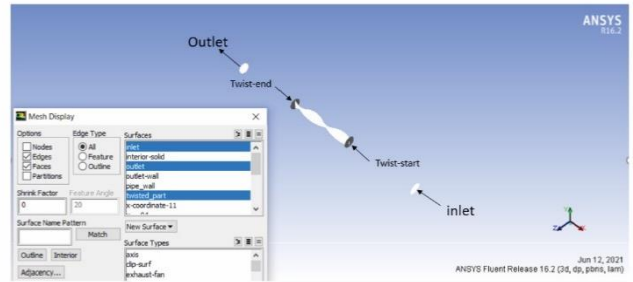
In this procedure, for Fig. 8, a random plain tube of 19.6 mm in length, a constant heat flux of $q=300 \text{ Wm}^{-2}$, and inlet temperature, $T_{inlet}= 306 \text{ K}$ were taken and water was used as fluid. The calculation of Nusselt Number and Heat Transfer Co-efficient is depicted below by those images.

From subordinate figure (a) of Fig. 8, it can be easily seen by using Ansys 16.2, the outlet plane has been was created by isosurface command. Then the following picture (b), the outlet wall surface has been originated by the help of isosurface command again. Before that outlet and pipe-wall i.e. fluid domain options have been selected simultaneously. Picture (c) presents the initial value of temperature 306K. In picture (d) and (e), the mass weighted temperature at the outlet wall for water flowing through the tube and other reference values of are shown. Following picture (f), selecting surface integral from Reports and area weighted average from the type of report, the outlet wall Nusselt number can be calculated by fixing the field variable option to wall fluxes. From picture (f), the Nusselt number is observed 4.393 which is close to the actual Nusselt number 4.36 in constant heat flux condition for any length of plain tube. The surface heat transfer co-efficient can also be

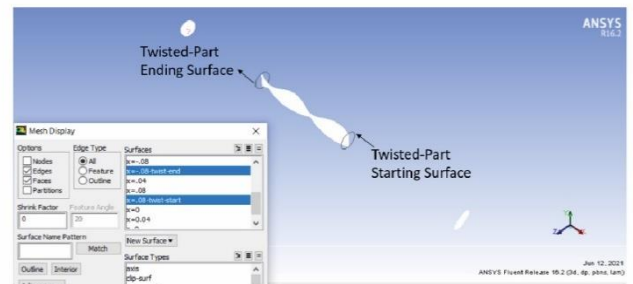
calculated by selecting the option surface heat transfer co-efficient shown in picture (g).



(a) Total fluid domain of tube



(b) Inlet-Outlet Plane and Twisted-Part



(c) Starting and Ending Surface Area of Twisted Part

Fig. 9 Twisted tape inserter starting, ending planes and surfaces

From Fig. 9, how the Nusselt number and heat transfer co-efficient in the twisted tape inserter are calculated can be easily visualized. In picture (a), the fluid domain and the direction of flow are represented. In the next picture (b), twist starting and ending planes have been created with the help of isosurface command. Twisted tape inserter's starting and ending surface have been originated same way as described previously in Fig. 8. By the temperature difference between the mass weighted averages of the twist starting and ending plane to the area weighted averages of the twist starting and ending surface, LMTD is calculated. From Equation 14 of section 3, the heat transfer co-efficient can be analyzed. Then, Equation 10 from section III, is utilized for measuring Nusselt number for various Reynolds numbers. From Fig. 9, how the Nusselt number and heat transfer co-efficient in the twisted tape inserter are calculated can be easily visualized. In picture (a), the fluid domain and the direction of flow are represented. In the next picture (b), twist starting and ending planes have been created with the help of isosurface command. Twisted tape inserter's starting and ending surface have been originated same way as described previously in Fig. 8. By the temperature difference between the mass weighted averages of the twist starting and ending plane to the area weighted averages of the twist starting and ending surface, LMTD is calculated. From Equation 14 of section 3, the heat transfer co-efficient can be analyzed.

Then, Equation 10 from section III, is utilized for measuring Nusselt number for various Reynolds numbers.

3.4 Mesh Independency Test and Model Validation

A series of simulations have been conducted for the mesh independence test. A different number of meshes were used to visualize the change in the heat transfer characteristics, i.e., Nusselt number in the plain tube with constant heat flux. A plain tube having constant heat flux possesses a Nusselt number 4.36 [36]. From Table 2, it is seen that mesh with element size 1.8 mm can produce almost similar results with meshes with element size 1.5 mm and 1 mm. Also, results just deviate 0.7% from the reference value, which is equal to 4.36. This mesh was used for further simulations.

Table 2 Mesh independency test

Element size	Nodes	Elements	Nusselt number
2.5 mm	44763	151347	4.4296
2 mm	79866	291358	4.4098
1.8 mm	103525	391318	4.3916
1.5 mm	163298	657043	4.391
1 mm	488808	2184342	4.3903

It is known that for the constant heat flux condition, the Nusselt number for a plain tube is 4.36 in case of any value of Reynolds number. From Fig. 7, it is observed that the numerical results with the element size 1.8-mm is 4.3916, which is close to the theoretical value for all the Re, taken in consideration. Another validation was done by comparing the experimental results conducted by L. Syam Sundar et al. using TiO₂ nanofluid in a plain tube with constant heat [13]. In that case, a simple tube having a length of 1.5 m, 0.005 ID, and 0.006 OD was used as geometry. As the numerical simulation ran based on constant heat flux, a constant heat flux of $q=4000 \text{ w m}^{-2}$, inlet temperature $T_{\text{inlet}}= 300\text{k}$, Reynolds number (Re) ranging from 300 to 2100 with an interval of 300 and TiO₂ nanofluid containing 0.3% volume fraction had been used. In this present study, the same values are taken to run the simulation and compare with the results of the existed values of L of Syam Sundar’s work which is shown in Fig. 11.

From Fig. 9, it is clearly observed that for Reynolds numbers ranging from 300 to 2100 for 0.3% volume fraction of TiO₂ nanofluid, the Nusselt number variation is minimal between the present work and L. Syam Sundar’s numerical results. At Reynolds number=300, Nusselt number is 6.52 for the current work, which is 6.44% higher than Sundar’s analysis. However, at a higher Reynolds number, this variation becomes relatively less. For example, at Reynolds number 900, the variation is 3.695%. Again, if the value of the Reynolds number being 1500 for the present state, the value of the Nusselt number is 11.04, and in Sundar’s explanation [13], it was observed 10.878, which is 1.467% lower than the present state. At higher Reynolds number 2100, this variation becomes to a minimum percentage which is equal to 0.862%. That means that the present work has been entirely accurate and close the simulation values for the same boundary conditions, illustrated by L. Syam Sundar et al.

[13]. Fig. 10 and Fig. 11 gave reasonably accurate results in the process of validation. The negligible deviations were eliminated for the conveniences in future procedures.

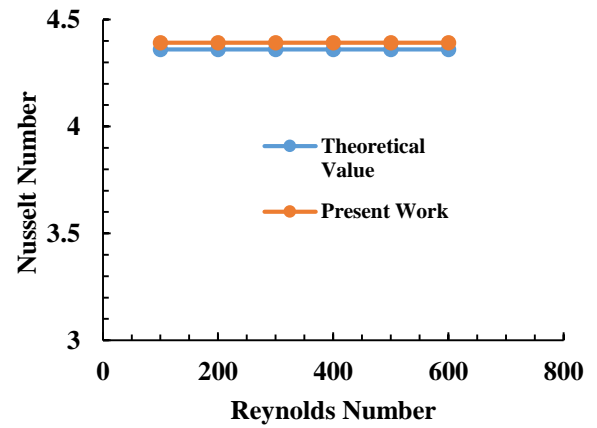


Fig. 10 Model validation for a plain tube having constant heat flux

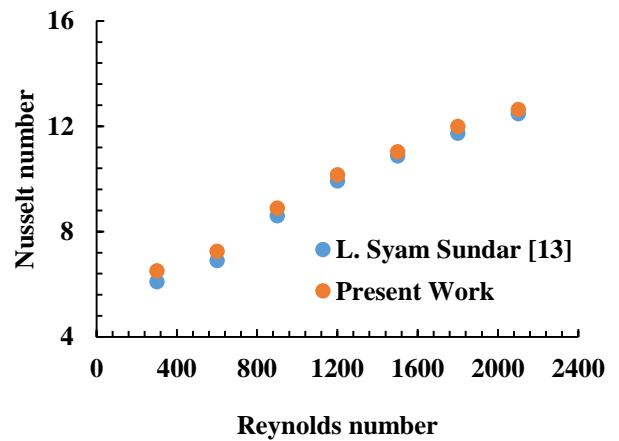


Fig. 11 Model validation for TiO₂ nanofluid flow through a tube with constant heat flux

4 Results and Discussions

The total core hour for the entire calculation is (4×28×24). Fig. 12 depicts temperature contour at the different cross-sections. As mentioned above, the length of the tube is 0.5 m. For this figure, the length of the twisted tape inserter 0.3 m has been taken and the twist ratio 3. The direction of flow is seen from section 2, Fig. 1. From Fig. 12, it is seen that the starting point of flow (0.0 m position) is the inlet of tube. It has not been considered in the contours because the change in flow pattern is mainly seen from the start of the twist i.e. at 0.1 m of tube. It is observed at 0.1 m, from sub-Fig (a), the temperature is lower than the other section of the tube because the mixing of fluid is about to start. Moving forward, at 0.15-m of tube, the temperature tends to increase in Fig (b). At the middle section of the tube, i.e., Fig (c), the change can be easily visualized. Same tendency is seen in Fig (d) and at the end of the twisted tape insert i.e. at 0.4-m tube length in Fig (e). Fig (f) represents the highest possible temperature is obtained at the outlet position of the tube. Fig (g) illustrates the flow has been thermally fully developed as the temperature reaches its peak value at the tube's ending or outlet.

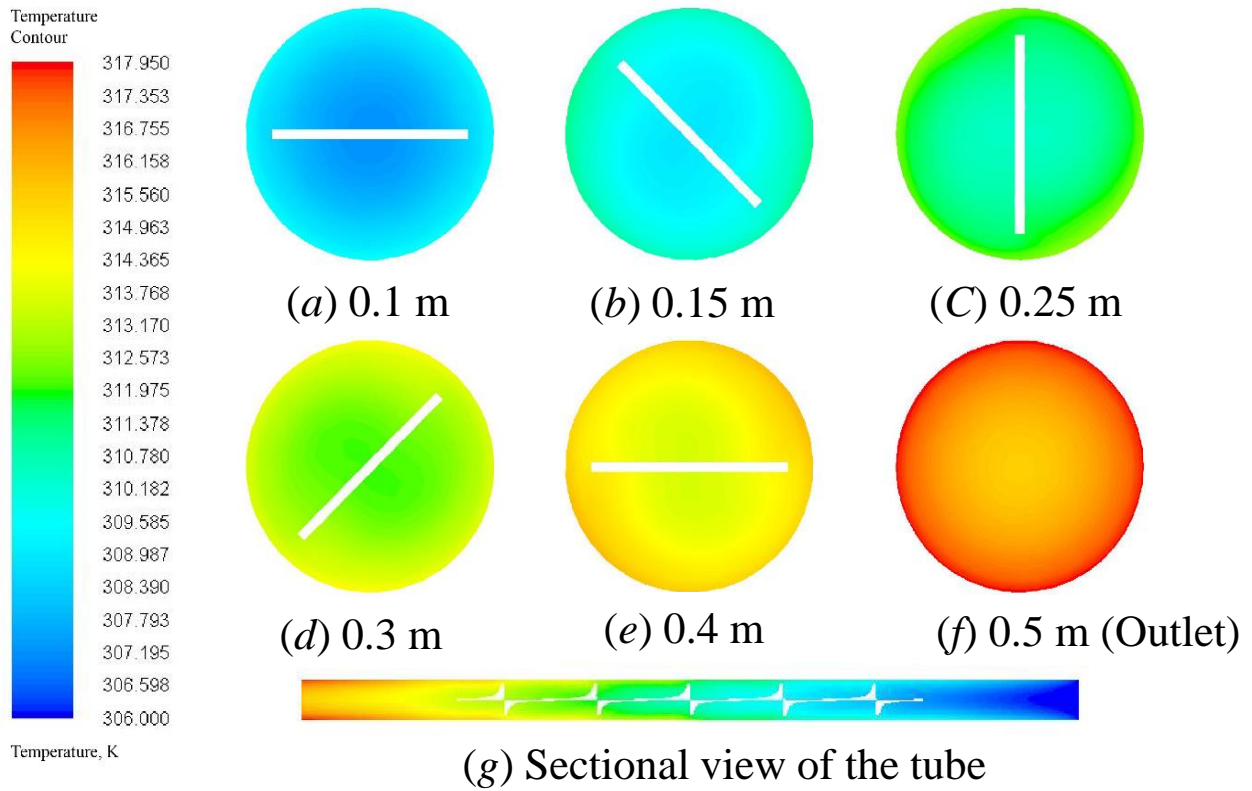


Fig. 12 Temperature contour at different sections whereas distance measure from the inlet

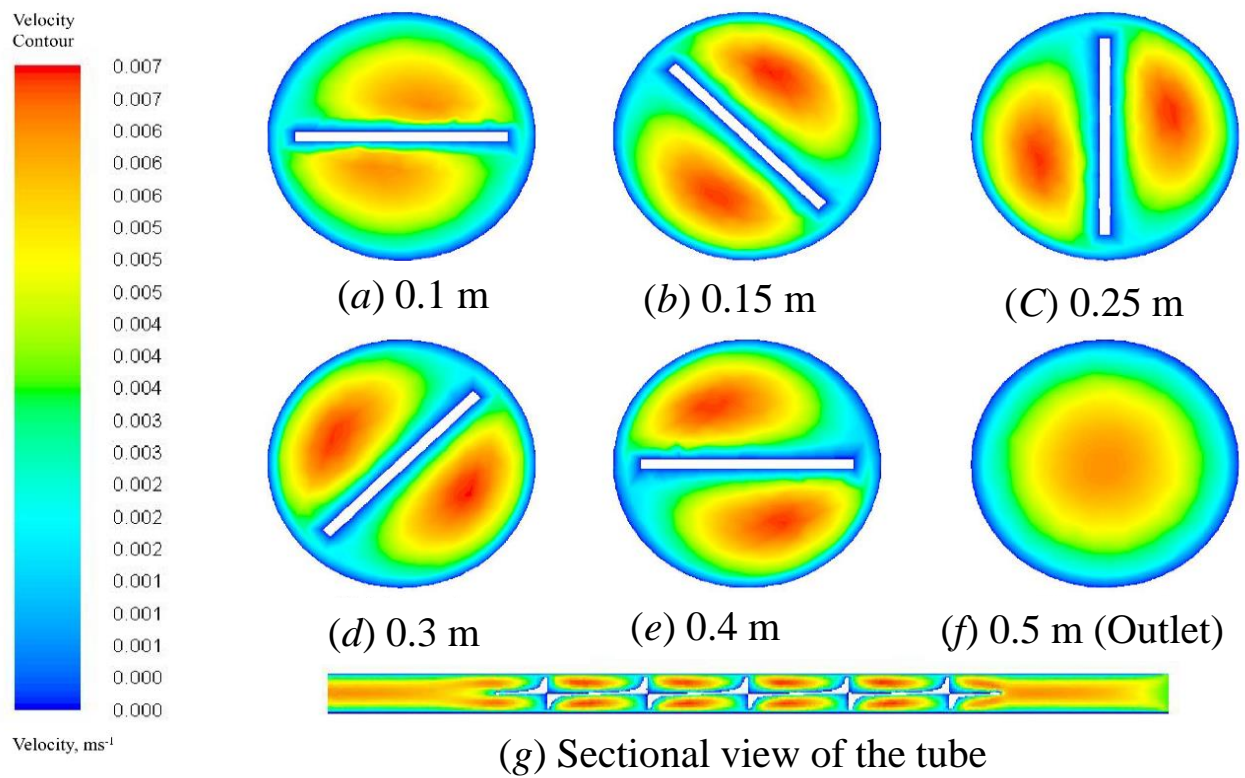


Fig. 13 Velocity contour at different cross-sections whereas distance measure from the inlet

In Fig. 13, same parameters are used just like Fig. 12. It is seen that the velocity of nanofluid flow tends to zero when the fluid is adjacent to the solid portion. Fig (a) depicts that the flow does not reach its maximum velocity at the 0.1 m distance of the tube, i.e., starting the twisted-tape. However, from Fig (b) to (e), for increasing linear distance, higher flow velocity is visualized for a specific portion, mainly at the centroid portion between the surface tube and the twisted part. Since the length of the twisted tape is 0.3-m, at the end of the twisted-tape, i.e., at 0.4 m of the tube, the highest possible velocity or peak velocity is observed because the velocity profile becomes fully developed. Fig (f) illustrates the outlet condition briefly in the pipe. As the flow became fully developed previously, there would not be any vital change in flow velocity characteristics, and subordinate Fig (g) reveals the flow is fully developed before reaching the outlet of the plain tube. The fully developed region's starting distance from inlet can be made analytically by entrance length formula which is described in Equation 16 from section 3.

The parameters related to heat transfer augmentation vary for changing specific parameters in the tube with twisted-tape insert. Twist ratio, Reynolds number, number of twists for a certain length twisted-tape, and volume fractions of fluid change the heat transfer parameters of fluid flow through a tube. Those parameters' impact on heat transfer characteristics both for water and nanofluid has been judged and illustrated. The most significant part of this paper investigates the changes of the stated features at the tube outlet and the twisted-tape part.

From Fig. 14, it is evident that the Nusselt number in the twisted-tape section is relatively higher than the value of the outlet wall section. The Nusselt number of twisted-tape section was calculated by creating isosurfaces both at the twist-start and end section, finding LMTD and heat transfer co-efficient within that section which is described elaborately in section 3 (Fig. 9). Since it is known the heat transfer rate at the twisted-tape section will be higher because of the higher fluid mixing, Nusselt number increment is visualized in the twisted tape portion than the outlet section. The highest possible Nusselt number at the outlet section and the twisted-tape will be gained for twist-ratio 1, Reynolds number (Re) 500 whereas the lowest is for twist-ratio 5, Reynolds number 100. The reason for this was judged previously. The maximum Nusselt number for the outlet wall section 6.975, whilst in the twisted-tape portion, it is 7.372. That shows the increment has gone 5.385%. Similarly, the lowest possible values at the outlet wall and the twisted-tape section are 4.423 and 5.1635. The percentage of enhancement in Nusselt number is 14.34. The reason for both increments can be explained by higher mixing of fluid in twisted area, extended surface area of twisted tape inserter and obstacle in boundary layer development. In the twisted tape section swirl flow happens. As the flow has gone fully developed at a certain distance, a slight change in fluid flow velocity happened by proceeding further. Most importantly, the higher mixing of fluid enhances the heat transfer rate and the heat transfer parameters.

From Fig. 15, it can be easily understood that the Nusselt number decreases at a higher twist-ratio. By varying the Reynolds number with the twist-ratio, the whole scenario is represented by the graph. For Reynolds number 100, 200, 300, 400 and 500 the decrease in Nusselt number at the outlet for twist ratio 1 to 5 is 10.4%, 16.07%, 18.67%, 20.7% and 23.832% respectively. The line for Reynolds number 500 shows linear decrement. This is due to the pitch of the twisted tape inserter decreases with the twist ratio. Thus, it is visualized that there will be more twists if the twist-ratio decreases and the mixing or turbulence of fluid would be higher for a certain length. Therefore, the Nusselt number shows an increment.

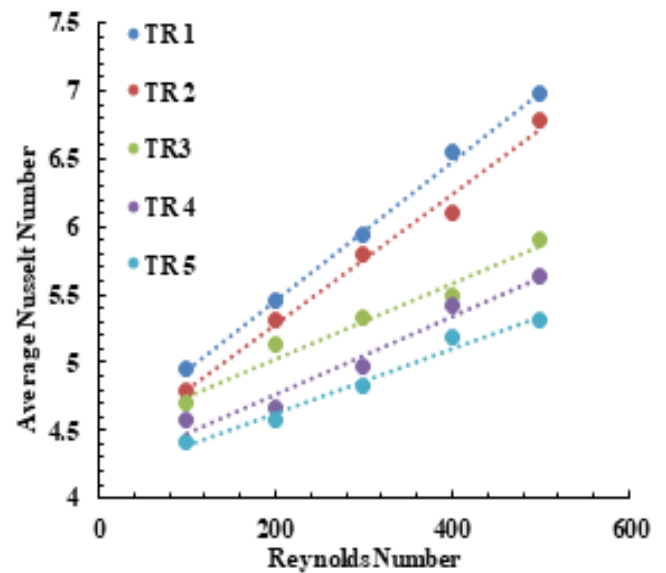


Fig. 14 Average Nusselt number vs. Reynolds number at the twisted-tape portion for water flowing through a tube for different twist ratios

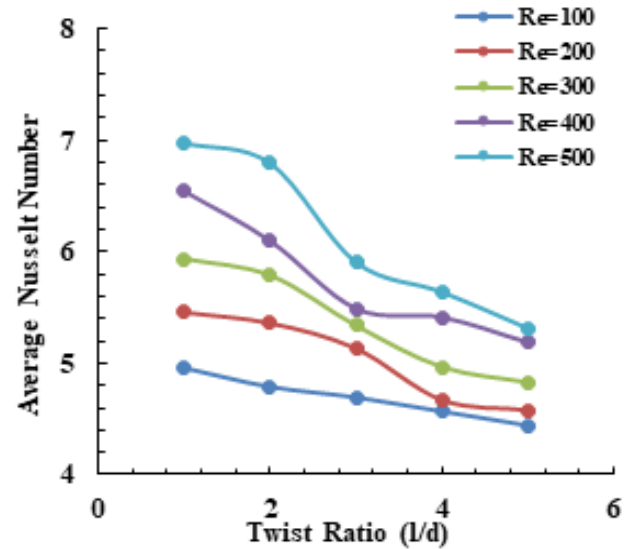


Fig. 15 Average Nusselt number vs. Twist ratio at the outlet wall for water flowing through a tube for different Reynolds numbers

It is revealed from Fig. 16, the 'highest' Nusselt number obtained for the twisted-tape portion is higher than the outlet wall section. This happens due to higher percentage mixing or turbulence and friction of fluid adjacent to the twisted tape inserter. Thus, the increased heat carrying capacity fluid of twisted portion leads to higher Nusselt number. At a certain distance of the tube, the flow becomes fully developed and this fully developed flow helps to generate the higher Nusselt number in the twisted tape inserter. And at the outlet, the fully developed flow remains steady. No turbulence is happened. That is the reason for lower Nusselt number at the outlet wall than the twisted tape portion. Like before, for Reynolds number 100, 200, 300, 400 and 500 the decrement in Nusselt number for twist ratio 1 to 5 in twisted-tape inserter is 18.5%, 17.22%, 18.77%, 19.21% and 20.265%. The decrement for twist-ratio 4 and 5 for all the Reynolds numbers is not high enough for the twisted-tape portion. This significant change is seen for twist ratios 1, 2, and 3 because of the more mixing of fluid and interruption in boundary layer development.

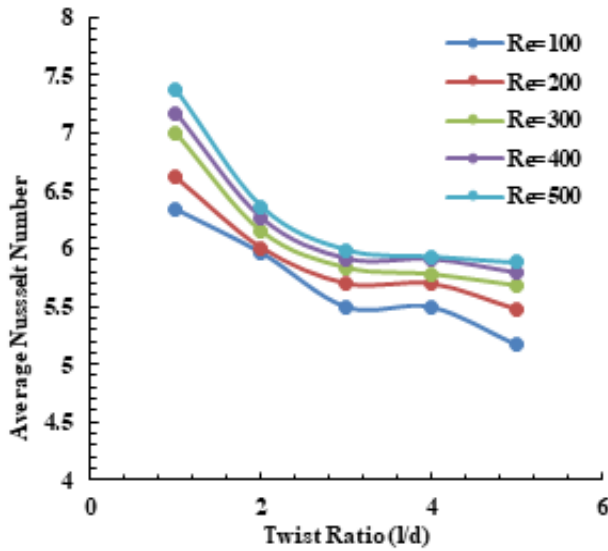


Fig. 16 Average Nusselt number vs. Twist ratio at the twisted-tape portion for water flowing through the tube for different Reynolds numbers

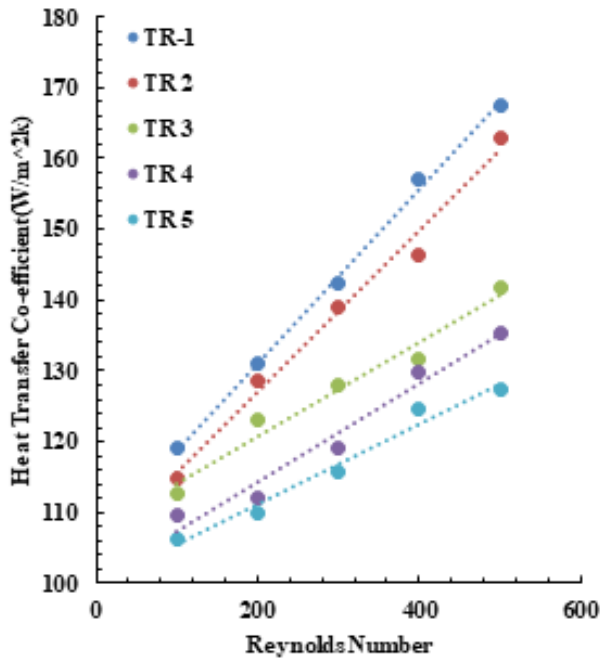


Fig. 17 Heat transfer co-efficient vs. Reynolds number at the outlet wall for different twist ratios for water flowing through the tube

From Fig. 17, it is evident that the heat transfer coefficient increases due to the increase in Reynolds number for any twist ratio. However, it shows the maximum possible value for twist ratio 1 and Reynolds number 500, 167.2. On the other hand, the lowest value is gained for twist ratio 5, and Reynolds number 100 that is 106.152. The percentage of increment is 36.58%, from the lowest to the highest value. If each twist ratio is separately considered, there will be 28.91%, 29.49%, 20.5%, 18.99%, and 16.75% increase in heat transfer co-efficient for twist ratio 1, 2, 3, 4, and 5 respectively. It is investigated that the increase is higher for twist ratios 1 and 2 than the rest. In contrast, this enhanced heat transfer rate drops quite linearly because of larger twist ratios as the fluid mixing decreased. From the trend lines, it can be easily understood the increment is linear for laminar flow for those parameters, i.e., Reynolds number and twist ratio.

As previously discussed, the heat transfer coefficient in the twisted-tape section is numerically analyzed by Ansys 16.2 software by creating isosurfaces at both ends of the twist. Then the LMTD was manually calculated within the twisted tape inserter portion. Constant heat flux is confined to the total plain tube, and the heat transfer co-efficient is analyzed just as discussed in section 3.3. From Fig. 18, it is seen that for twist ratios 4 and 5, the heat transfer increases linearly in small percentage. The percentages of increment are 11.762 and 12.155, respectively. On the other hand, for twist ratios 1, 2, and 3, the increment in rate is 14.02, 6.29, and 8.248% according to for Reynolds number 100 to 500. The maximum and minimum values are for Reynolds number 500, twist ratio 1 and Reynolds number 100, twist ratio 5. Compared with the outlet section, an increment of heat transfer coefficient at the twisted-tape portion is seen because the fluid flow gets much barrier at the twisted-tape section than the outlet wall as swirl flow created in the area for extended surface area. After passing through this section, the flow becomes fully developed, and a slight change in flow rate has been visualized.

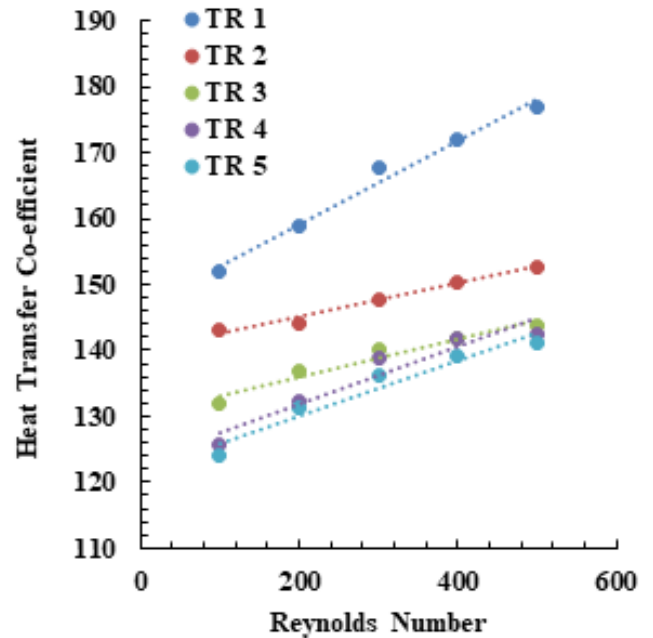


Fig. 18 Heat transfer co-efficient vs. Reynolds number at the twisted-tape section for different twist ratios for water flowing through the tube

From Fig. 19, it is evident that in this graphical representation, twist ratio has taken as an independent parameter. The presence of twisted tape inserter augments the heat transfer rate which is explained by the Equation 12 in section 3. The decrement is seen for the increased twist ratio. For twist ratio 1 to 5 the decrement is 10.79%, 16.05%, 18.67%, 20.7% and 23.8% for the described Reynolds numbers. The trend line quite similar to Fig. 15.

As discussed previously, the twisted inserter's heat transfer co-efficient was numerically investigated with the LMTD of the twisted tape's starting and ending planes (section 3.3). This passive technique of enhancing heat transfer increases the compactness of the inserter with extended surface area. These pathways of the twisted tape lead to high pressure drop. Pressure drop depends on fluid velocity; change in velocity field near twisted-tape wall will eventually increase the heat transfer co-efficient. At the extended surface area, there will be boundary layer development.

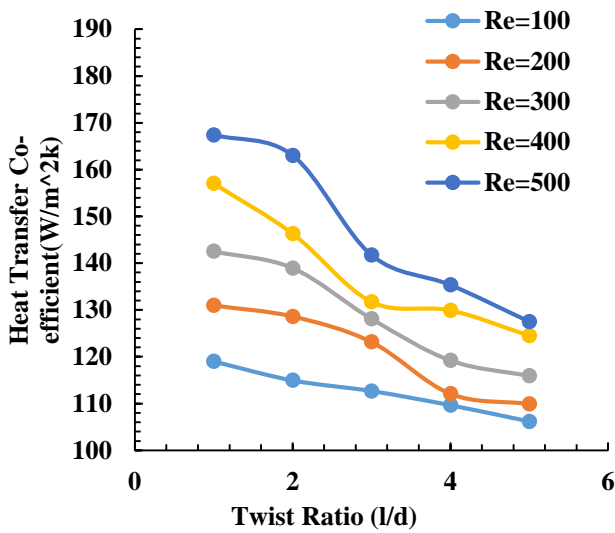


Fig. 19 Heat transfer co-efficient vs. twist ratio at the outlet wall for different twist ratios for water flowing through the tube

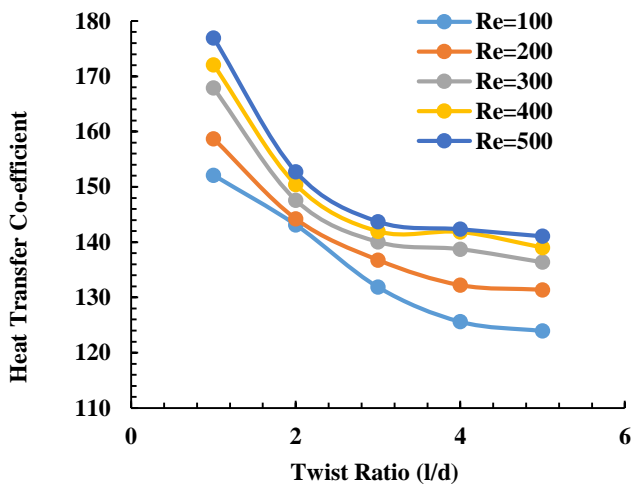


Fig. 20 Heat transfer co-efficient vs. twist ratio at the twisted-tape for different twist ratios for water flowing through the tube

As the tapes are small, boundary layer cannot develop infinitely and hence, faces obstacles continuously. Therefore, heat transfer co-efficient increases at the twisted tape portion. On the other hand, near the outlet wall of the tube, the flow becomes steady. In Fig 19, a less sharp decrease in heat transfer co-efficient is observed at that section because the flow has already become fully developed. No change in velocity field is evident. For twist ratios 4 and 5, the change in that parameter is not significant enough. It stays in a pretty stable situation for the described Reynolds numbers instead. In case of the twist ratios 1, 2, and 3, the change is significant for the Reynolds number 100 to 500. The percentages of variation between twist ratios 1 and 3 for Reynolds number 100 to 500 are 13.31, 13.836, 15.455, 17.51, and 18.77%. As the mixing of fluid becomes lower with the increase in twist ratio, heat transfer co-efficient encounters a decrement trend, illustrated by Fig. 20.

From Fig. 21, it is evident that for twist ratios 1, 2, and 3, the pressure drop per meter length of the twisted-tape portion has little difference, which can be seen from the trend line equations. For twist ratios 1 and 2, the ‘pressure drop’ changes pretty significantly in any Reynolds number. In both aspects, i.e., twist ratio 1 and 2, there is an increase of 22.78%, 25.53%, 29.95%, 33.82%, and 36.895% in pressure drop, respectively for Reynolds number 100 to 500. Thus, by decreasing twist-ratio,

higher pressure drop can be obtained for any Reynolds number in laminar flow.

If a certain length of twisted-tape is taken for investigating the effect of the number of twists on heat transfer characteristics in a tube, for instance, by taking multiple twists, significant changes can be visualized in heat transfer phenomena at the outlet wall and the twisted-tape portion of that tube.

From Fig. 22, it is seen for the increased number of twists in a certain length the Nusselt number increases. In this particular case, the length of the twisted-tape was taken at 0.3 m. It had twists number 1,2,3,4 and 5 for a specific Reynolds number 100. Both for the outlet wall and the twisted-tape inserter Nusselt number increases quite linearly, which is observed from the figure above and the trend lines. The calculation of Nusselt number at outlet wall and twisted-tape inserter portion was discussed previously. The twisted tape portion provides higher values because the mixing, velocity and heat carrying capacity are higher in this section, which is also illustrated.

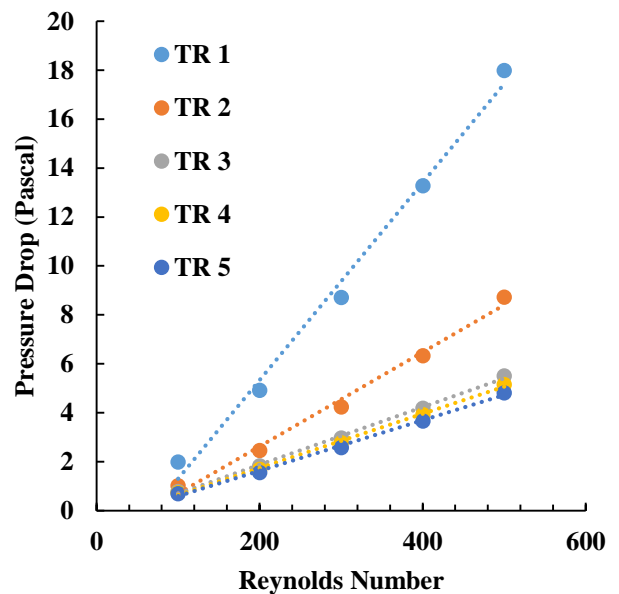


Fig. 21 Pressure drop vs. Reynolds number at the twisted-tape for different twist ratios for water flowing through the tube

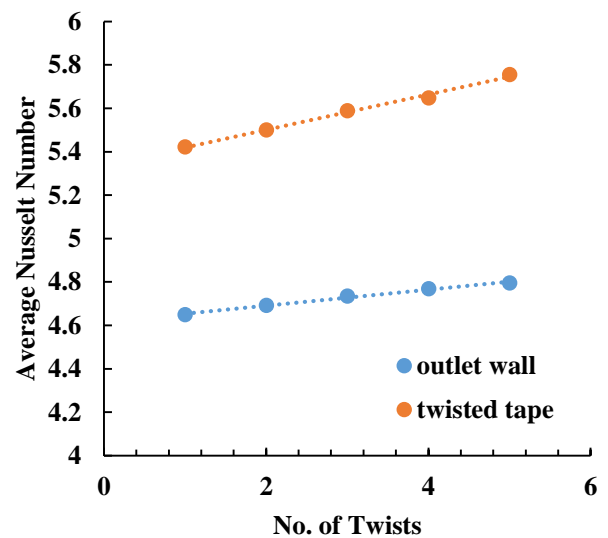


Fig. 22 Graphical representation of Average Nusselt number vs. no. of twists at the outlet wall and twisted tape for water flowing through the tube

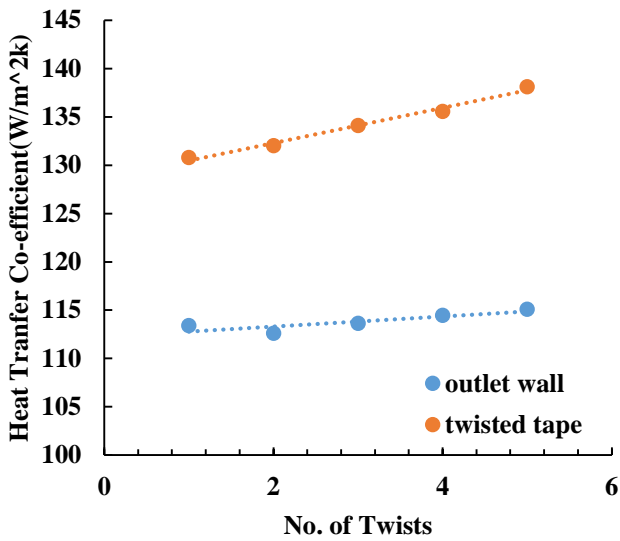


Fig. 23 Graphical representation of heat transfer co-efficient vs. no. of twists at the outlet wall and twisted tape for water flowing through the tube

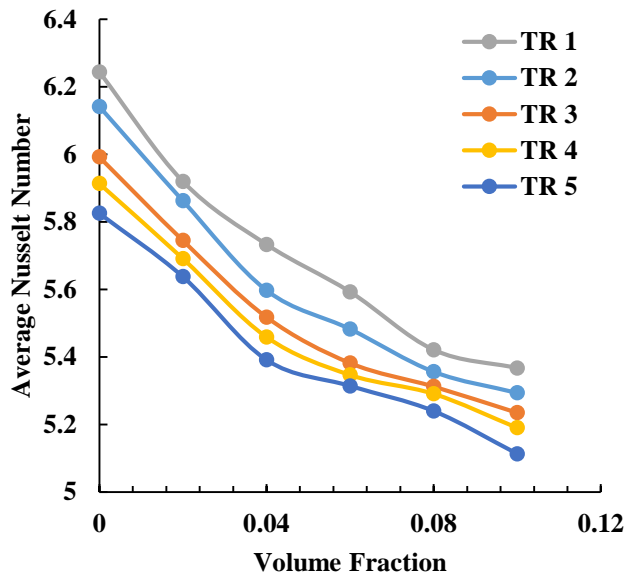


Fig. 24 Average Nusselt number vs. volume fractions at the outlet wall for different twist ratios

As stated previously, if the number of twists increases for a certain length, the heat transfer coefficient also increases. The reason behind this is for increasing the number of twists, the pitch length decreases. Thus, the twist ratio also faces a decrement. All those reasons combined are responsible for heat transfer augmentation, i.e., increasing in heat transfer co-efficient. From Fig. 23, difference in heat transfer coefficient in the twisted-tape portion and outlet wall at the tube can be described. Considering the same values discussed in Fig. 22, the heat transfer coefficient represents the linear increment in both outlet wall and twisted-tape portions. By taking twist numbers 1 to 5 for 0.3 m twisted tape inserter and Reynolds number 100, the increased percentage of heat transfer co-efficient for the twisted tape inserter portion than the outlet wall are seen 13.3 %, 14.71 %, 15.27 %, 15.57 % and 16.68 % respectively.

For nanofluid (TiO₂+water) flow through the tube, there is seen quite a few changes in terms of heat transfer characteristics as the volume fractions of nanofluid change. In this paper, five different volume fractions have been taken to judge the variation in heat transfer phenomena. From Fig. 24, it can be clearly

understood that for twist ratio 1 and volume fraction 0, the highest Nusselt number is obtained, which values 6.244. The lowest value is acquired for the highest twist ratio 5, volume fraction 0.1, which is 5.1128. All the values obtained have been calculated for Reynolds number 100. Most importantly, this figure shows similarity for any twist ratio. If the volume fraction of nanofluid increases, the Nusselt number decreases. This decrement rate is approximately close in all cases. For twist ratio 1 to 5 and volume fractions 0 to 0.1 with an interval of 0.02, the decrement percentage is 14.04, 13.8, 12.63, 12.23, and 12.22 respectively for the stated conditions.

The Fig. 25 shows that the increased volume fractions of nanofluid flow in a twisted-tape causes increment in heat transfer co-efficient. As the numerical value of volume fraction increases, heat transfer co-efficient also reaches its peak. At the outlet wall, the highest value is 343.987 for volume fraction 0.1, twist ratio 1, whereas the lowest value provided by Ansys 16.2 software is 137.761 for twist ratio 5. Both values are judged under the condition of Reynolds number 100. For water, the same procedure was done in Fig. 17, where the highest and lowest value of heat transfer coefficients are 106.152 and 118.992 for Reynolds number 100. Thus, it can be said by adding particles in fluid flow, a higher heat transfer augmentation happens in the same boundary conditions. This occurs due to higher mixing of nanofluid and swirling phenomena at the twisted-tape section. The above graph illustrates that the increment in heat transfer co-efficient is linear which can be acknowledged by the trend lines.

From above figures relating to the nanofluid flow, a significant difference is visualized between water and nanofluid flow through the plain tube in the same boundary conditions. For water flows through the tube, both the Nusselt number and heat transfer co-efficient face a significant increase. However, in the case of TiO₂ nanofluid flow for the stated parameters, a decline in the values of Nusselt number is seen. On the other hand, a significantly higher heat transfer coefficient is obtained. This phenomena describes the nanofluid flow's main characteristics.

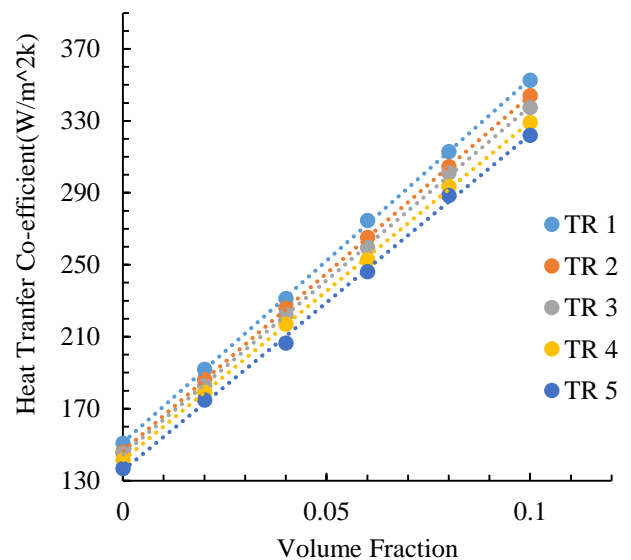


Fig. 25 Heat transfer co-efficient vs. volume fractions at the outlet wall of the twisted-tape inside the pipe containing nanofluid (TiO₂+water)

In the case of pressure drop, a decline with the increase in volume fractions can be easily visualized. From Fig. 26, it is evident that the decrement is linear for all the twist ratios and volume fractions. For water, the pressure drop per meter length is relatively higher, which is illustrated elaborately in Fig. 21.

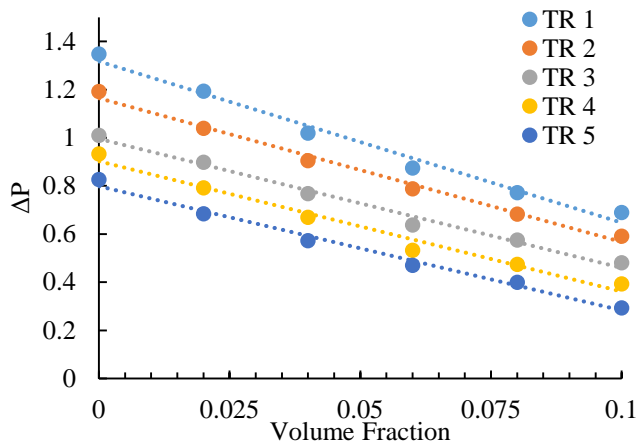


Fig. 26 Pressure drop vs. volume fractions at the twisted-tape section inside the pipe containing nanofluid (TiO₂+water)

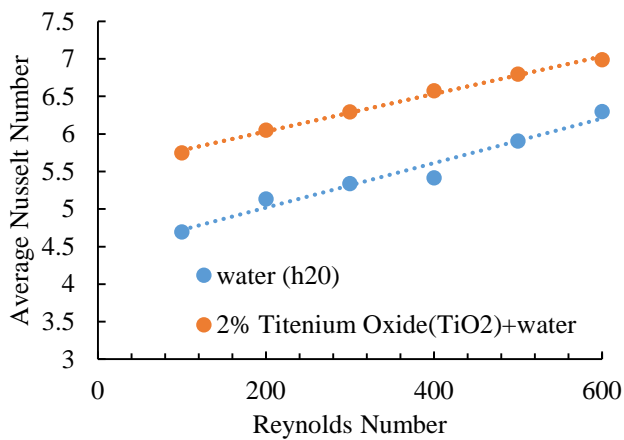


Fig. 27 The Nusselt number between water and nanofluid flowing through the tube for different Reynolds numbers at the outlet wall

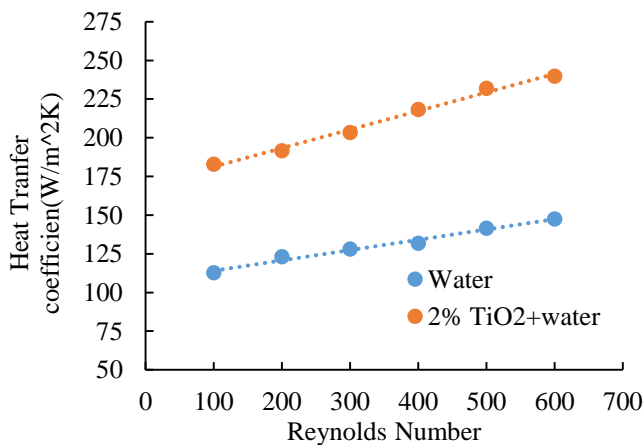


Fig. 28 The heat transfer coefficient between water and nanofluid flowing through the tube for different Reynolds numbers at the outlet wall

However, in Fig. 26, the values of pressure drop obtained in nanofluid flow are much less. For twist ratios 1 to 5 and volume fractions 0 to 0.1 with an interval of 0.02, a decrease of 48.83 %, 50.4 %, 52.475 %, 57.976 %, and 64.45 % ‘pressure drop’ is obtained from highest value to the lowest (considering Re=100). From the trend lines, it is evident that this decline phenomena regarding the stated parameters is linear.

Fig. 27 illustrates the variation in Nusselt number for water and TiO₂ nanofluid (2%) flow through the tube where Reynolds number 100 to 600 and a specific twist ratio 3 have been taken into consideration. It is evident that by increasing the Reynolds number, the Nusselt number increases both for water and nanofluid. By using 2% volume fraction of nano-fluid, the Nusselt number at the outlet wall increases 18.28 % for Re=100, 15.18 % for Re=200, 15.189 % for Re=300, 17.644 % for Re=400, 13.12 % for Re=500 and 9.945 % for Re=600. Thus, the difference can be easily comprehended by the stated boundary conditions and graphical representation. Not only for twist ratio 3 but also for other twist ratios and volume fractions, this difference will be observed if any analytical description is made. From Fig. 28, it can be easily understood that just like the Nusselt number, the heat transfer coefficient at the outlet wall, also shows an increment by increasing the value of Reynolds number. For water flow, the highest value is 147.529, whereas 2% TiO₂ nanofluid flow shows 239.872. A 38.49% increase at the outlet wall for Reynolds number 600 is obtained using nanofluid which is depicted in the graph. Same as Fig. 27, twist ratio 3 has been taken in this case. Reynolds number 100, 200, 300, 400 and 500 show 38.42%, 35.69%, 37.021%, 39.644% and 42.277% higher values than water flow at the outlet wall. An enhancement in heat transfer coefficient is clearly seen for all the twist ratios if nanofluid is used instead of water through the plain tube.

5 Conclusion

A comprehensive investigation of convective heat transfer through a circular pipe consisting of a twisted tape inserter is presented. The analysis shows the enhancement in heat transfer phenomena due to nanofluid flow instead of pure fluids. The parameters investigated in this procedure are volume fraction, twist ratio, number of twists, and the Reynolds number. The result clearly shows that the amount of heat transfer coefficient is increased with the increase in volume fraction of nanoparticles. However, the Nusselt number decreases with the increment in fractional volume. In another case, Nusselt number increased with a decrease in twist ratio from 5 to 1. Beyond this, it is found that maximum heat transfer is obtained at twist ratio one. The quantity of heat transfer and Nusselt number is increased with the increase in Reynolds number. Increasing the number of twists for a specific length of twisted tape depicts if the twist becomes more than one for this length, the pitch length decreases. Hence, the heat transfer coefficient, and Nusselt number increase. Differences between water flow and nanofluid flow by taking two heat transfer augmentation parameters, i.e., Nusselt number and heat transfer coefficient at the tube's outlet wall have been depicted. Not only at the outlet wall but also at the twisted-tape portion, the differences among heat transfer parameters were illustrated elaborately both for water and TiO₂ nanofluid flow. All numerical analyses, including different heat transfer parameters for nanofluid flow, were numerically calculated by taking the particles' size 10 nm. Greater sizes could also be taken, but the simulations for investigating will be time-consuming. In the tables and graphical representations, the values were compared percentage-wise in the paper. By trend lines, it was easy to comprehend the change in each aspect of specific heat enhancement characteristics.

This work could be further extended by using a double twisted-tape and investigating those stated effects at higher Reynolds numbers.

Nomenclature

l = length of the pitch
 d = width of the tube
 T, R = Twist ratio (l/d)
 T = temperature (K)
 g = gravitational acceleration (ms^{-2})
 Nu = Nusselt number
 Re = Reynolds number
 h = heat transfer co-efficient ($\text{Wm}^{-2}\text{K}^{-1}$)
 ν = kinematic viscosity (m^2s^{-1})
 μ = dynamic viscosity ($\text{kgm}^{-1}\text{s}^{-1}$)
 ρ = density (kgm^{-3})
 ψ = stream function (m^2s^{-1})
 k = thermal conductivity ($\text{Wm}^{-1}\text{K}^{-1}$)
 C_p = specific heat ($\text{Jkg}^{-1}\text{k}^{-1}$)
 Φ = volume fraction
 q = constant heat flux (Wm^{-2})

References

- [1] Somerscales, E.F. and Bergles, A.E., 1997. Enhancement of heat transfer and fouling mitigation. *Advances in heat transfer*, 30, pp.197-253.
- [2] Eldabe, N.T., Abo-Seida, O.M., Abo-Seliem, A.A., ElShekhiy, A.A. and Hegazy, N., 2017. Peristaltic transport of magnetohydrodynamic carreau nanofluid with heat and mass transfer inside asymmetric channel. *American Journal of Computational Mathematics*, 7(01), p.1-20.
- [3] Sundar, L.S., Singh, M.K. and Sousa, A.C., 2014. Enhanced heat transfer and friction factor of MWCNT–Fe₃O₄/water hybrid nanofluids. *International Communications in Heat and Mass Transfer*, 52, pp.73-83.
- [4] He, W., Toghraie, D., Lotfipour, A., Pourfattah, F., Karimipour, A. and Afrand, M., 2020. Effect of twisted-tape inserts and nanofluid on flow field and heat transfer characteristics in a tube. *International Communications in Heat and Mass Transfer*, 110, p.104440.
- [5] Arulprakasajothi, M., Elangovan, K., Reddy, K.H.C. and Suresh, S., 2016. Experimental investigation on heat transfer effect of conical strip inserts in a circular tube under laminar flow. *Frontiers in Energy*, 10(2), pp.136-142.
- [6] Eiamsa-ard, S., Wongcharee, K., Eiamsa-Ard, P. and Thianpong, C., 2010. Heat transfer enhancement in a tube using delta-winglet twisted tape inserts. *Applied Thermal Engineering*, 30(4), pp.310-318.
- [7] Peng, Y., Alsagri, A.S., Afrand, M. and Moradi, R., 2019. A numerical simulation for magnetohydrodynamic nanofluid flow and heat transfer in rotating horizontal annulus with thermal radiation. *RSC advances*, 9(39), pp.22185-22197.
- [8] Chang, S.W., Yu, K.W. and Lu, M.H., 2005. Heat transfers in tubes fitted with single, twin, and triple twisted tapes. *Experimental Heat Transfer*, 18(4), pp.279-294.
- [9] Eiamsa-ard, S., Wongcharee, K., Kunnarak, K., Kumar, M. and Chuwattabakul, V., 2019. Heat transfer enhancement of TiO₂-water nanofluid flow in dimpled tube with twisted tape insert. *Heat and Mass Transfer*, 55(10), pp.2987-3001.
- [10] Jafaryar, M., Sheikholeslami, M. and Li, Z., 2018. CuO-water nanofluid flow and heat transfer in a heat exchanger tube with twisted tape turbulator. *Powder technology*, 336, pp.131-143.
- [11] Kumar, B., Kumar, M., Patil, A.K. and Jain, S., 2019. Effect of V cut in perforated twisted tape insert on heat transfer and fluid flow behavior of tube flow: an experimental study. *Experimental Heat Transfer*, 32(6), pp.524-544.
- [12] Meyer, J.P. and Abolarin, S.M., 2018. Heat transfer and pressure drop in the transitional flow regime for a smooth circular tube with twisted tape inserts and a square-edged inlet. *International Journal of Heat and Mass Transfer*, 117, pp.11-29.
- [13] Syam Sundar, L., Sharma, K.V., Parveen, S. and Gaffar, M.A., 2009. Laminar convective heat transfer of nanofluids in a circular tube under constant heat flux. *International Journal of Nanoparticles*, 2(1-6), pp.314-320.
- [14] Haq, R.U., Noor, N.F.M. and Khan, Z.H., 2016. Numerical simulation of water based magnetite nanoparticles between two parallel disks. *Advanced Powder Technology*, 27(4), pp.1568-1575.
- [15] Celen, A., Kayaci, N., Çebi, A., Demir, H., Dalkılıç, A.S. and Wongwises, S., 2014. Numerical investigation for the calculation of TiO₂-water nanofluids' pressure drop in plain and enhanced pipes. *International Communications in Heat and Mass Transfer*, 53, pp.98-108.
- [16] Qi, C., Liu, M., Luo, T., Pan, Y. and Rao, Z., 2018. Effects of twisted tape structures on thermo-hydraulic performances of nanofluids in a triangular tube. *International Journal of Heat and Mass Transfer*, 127, pp.146-159.
- [17] Selimefendigil, F. and Öztop, H.F., 2016. Conjugate natural convection in a cavity with a conductive partition and filled with different nanofluids on different sides of the partition. *Journal of Molecular Liquids*, 216, pp.67-77.
- [18] Sheikholeslami, M., Ganji, D.D. and Rashidi, M.M., 2016. Magnetic field effect on unsteady nanofluid flow and heat transfer using Buongiorno model. *Journal of Magnetism and Magnetic Materials*, 416, pp.164-173.
- [19] Sundar, L.S., Kumar, N.R., Naik, M.T. and Sharma, K.V., 2012. Effect of full length twisted tape inserts on heat transfer and friction factor enhancement with Fe₃O₄ magnetic nanofluid inside a plain tube: An experimental study. *International Journal of Heat and Mass Transfer*, 55(11-12), pp.2761-2768.
- [20] Ternik, P., 2015. Conduction and convection heat transfer characteristics of water–Au nanofluid in a cubic enclosure with differentially heated side walls. *International Journal of Heat and Mass Transfer*, 80, pp.368-375.
- [21] Vashistha, C., Patil, A.K. and Kumar, M., 2016. Experimental investigation of heat transfer and pressure drop in a circular tube with multiple inserts. *Applied Thermal Engineering*, 96, pp.117-129.
- [22] Heris, S.Z., Nassan, T.H., Noie, S.H., Sardarabadi, H. and Sardarabadi, M., 2013. Laminar convective heat transfer of Al₂O₃/water nanofluid through square cross-sectional duct. *International Journal of Heat and Fluid Flow*, 44, pp.375-382.

- [23] Akbari, M., Behzadmehr, A. and Shahraki, F., 2008. Fully developed mixed convection in horizontal and inclined tubes with uniform heat flux using nanofluid. *International Journal of Heat and Fluid Flow*, 29(2), pp.545-556.
- [24] Rashidi, M.M., Nasiri, M., Khezerloo, M. and Laraqi, N., 2016. Numerical investigation of magnetic field effect on mixed convection heat transfer of nanofluid in a channel with sinusoidal walls. *Journal of Magnetism and Magnetic Materials*, 401, pp.159-168.
- [25] Barzegarian, R., Moraveji, M.K. and Aloueyan, A., 2016. Experimental investigation on heat transfer characteristics and pressure drop of BPHE (brazed plate heat exchanger) using TiO₂-water nanofluid. *Experimental Thermal and Fluid Science*, 74, pp.11-18.
- [26] Sun, F., Yao, Y., Chen, M., Li, X., Zhao, L., Meng, Y., Sun, Z., Zhang, T. and Feng, D., 2017. Performance analysis of superheated steam injection for heavy oil recovery and modeling of wellbore heat efficiency. *Energy*, 125, pp.795-804.
- [27] Naphon, P., Wiriyasart, S. and Arisariyawong, T., 2018. Artificial neural network analysis the pulsating Nusselt number and friction factor of TiO₂/water nanofluids in the spirally coiled tube with magnetic field. *International Journal of Heat and Mass Transfer*, 118, pp.1152-1159.
- [28] Akbari, O.A., Toghraie, D., Karimipour, A., Marzban, A. and Ahmadi, G.R., 2017. The effect of velocity and dimension of solid nanoparticles on heat transfer in non-Newtonian nanofluid. *Physica E: Low-Dimensional Systems and Nanostructures*, 86, pp.68-75.
- [29] Bas, H. and Ozceyhan, V., 2014. Optimization of parameters for heat transfer and pressure drop in a tube with twisted tape inserts by using Taguchi method. *Arabian Journal for Science and Engineering*, 39(2), pp.1177-1186.
- [30] Minea, A.A., Buonomo, B., Burggraf, J., Ercole, D., Karpaiya, K.R., Di Pasqua, A., Sekrani, G., Steffens, J., Tibaut, J., Wichmann, N. and Farber, P., 2019. NanoRound: A benchmark study on the numerical approach in nanofluids' simulation. *International Communications in Heat and Mass Transfer*, 108, p.1-23.
- [31] Lodhi, M.S., Sheorey, T. and Dutta, G., 2020. Single-phase fluid flow and heat transfer characteristics of nanofluid in a circular microchannel: Development of flow and heat transfer correlations. *Proceedings of the Institution of Mechanical Engineers, Part C: Journal of Mechanical Engineering Science*, 234(18), pp.3689-3708.
- [32] White, F. M., 1998, *Fluid Mechanics*, McGraw-Hill Higher Education.
- [33] Hatami, M., Kheirkhah, A., Ghanbari-Rad, H. and Jing, D., 2019. Numerical heat transfer enhancement using different nanofluids flow through venturi and wavy tubes. *Case Studies in Thermal Engineering*, 13, p.1-10.
- [34] Munson, B. R., Young, D. F., Okiishi, T. H. and Huebsch, W. W., 2015, *Fundamentals of Fluid Mechanics*, John Wiley & Sons, Inc., New Jersey.
- [35] Sakinah, S.Z.A., Azmi, W.H. and Alias, J., 2020, May. Characterization of TiO₂ nanopaint for automotive application. In *IOP Conference Series: Materials Science and Engineering* (Vol. 863, No. 1, p. 012053). IOP Publishing.
- [36] Holman, J. P. and Bhattacharyya, S., 2016, *Heat Transfer (In SI Units)*, Tata McGraw Hill Education Private Limited, New Delhi.